Self-Assembled Polymer Nanocomposites and Their Networks

ARTICLE *in* JOURNAL OF APPLIED POLYMER SCIENCE · NOVEMBER 2014

Impact Factor: 1.77 · DOI: 10.1002/app.41111

3 AUTHORS, INCLUDING:

Nitin Patil

University of Massachusetts Amherst

4 PUBLICATIONS **10** CITATIONS

Journal of Applied Polymer Science

Self-Assembled Polymer Nanocomposites and Their Networks

Nitin Patil, Jarred Kelsey, Jeffery L. White
Department of Chemistry, Oklahoma State University, Stillwater, Oklahoma 74078
Correspondence to: J. L. White (E-mail: jeff.white@okstate.edu)

ABSTRACT: Synthetic modifications to block-copolymer structure-directing agents lead to polymerizable macromers suitable for templating the growth of mesoporous silica particles, which can subsequently react *in situ* to form extended nanocomposites and nanocomposite networks. Suitably functionalized triblock polymers can preserve the structure-directing capabilities of the triblock polymer for templating ordered mesoporous silica particle growth and also generate a reactive matrix for subsequent polymer network formation via the reactive end groups. The final self-assembled products are polymer nanocomposites or novel crosslinked nanocomposite networks whose organic/inorganic composition ratios can vary systematically. The novel self-assembly route described here should be generally applicable to the synthesis of intimately mixed nanocomposites and nanocomposite networks, starting from a wide variety of block polymeric template/macromer/ordered silica systems. © 2014 Wiley Periodicals, Inc. J. Appl. Polym. Sci. **2014**, *131*, 41111.

KEYWORDS: amorphous; composites; crosslinking; porous materials

Received 17 April 2014; accepted 30 May 2014
DOI: 10.1002/app.41111

INTRODUCTION

Mesoporous silicas have received significant attention in material science because of their high surface area and highly ordered framework.[1–3] Interesting applications of mesoporous silica to materials design may arise by filling the pores of mesoporous silica with polymer,[4–9] and connecting those filled particles, to form nanocomposites. Solution or melt blending is the conventional and low-cost method for synthesizing polymer composites.[10–12] However, this method neither ensures homogenous distribution of the inorganic phase in high-molecular-weight polymers nor allows high-molecular-weight polymers to homogeneously fill the mesopores.

Two synthetic methodologies that can potentially address these limitations are postsynthetic grafting and co-condensation. Grafting is generally carried out by reacting the mesoporous silica silanol groups with an organosilane $(R'O)_3SiR$ (R being monomeric unit), followed by polymerizing the monomeric unit.[13–17] This limitation of this method is the homogenous distribution of polymer throughout the pores when the organosilanes react at the pore opening of the silica.[18] Co-condensation is a one-pot synthesis process where the ordered "crystallization" of the siliceous source (tetraethylorthosilicate) with terminal trialkoxysilanes $(R'O)_3SiR$ occurs in the presence of structure-directing agents, thereby generating organic-functionalized mesoporous silica.[7,18–21] By polymerizing the organic groups, polymer nanocomposites can be obtained. Both of these methodologies focus on anchoring monomeric group either after or during mesoporous silica synthesis via organosilane reagents. In a sol–gel process, the inorganic phase such as silica can be homogenously distributed in the polymer matrix from sol–gel reactions of tetraalkoxysilanes in the presence of reactive monomers or macromers.[18,22–27]

Here, we detail the end-group functionalization of the Pluronic®-based copolymers to attach either one or two reactive end groups, which in this case are either allyl- or acrylate-based as shown in Scheme 1. Allyl and acrylate reactive groups were selected because the vinyl groups in either case can be polymerized via free radical mechanism. Based on the choice of end group, final products can be made which are either (1) nanocomposites that contain only physical chain entanglements or (2) chemically crosslinked nanocomposite networks. In either case, the organic to inorganic composition ratios may be systematically varied in the final materials, as shown by several chemical, spectroscopic, and microscopic characterization methods described herein. The following sections will describe the polymeric surfactant functionalization chemistry, templating and growth of ordered mesoporous SBA-type silica using the modified surfactants, reactions of the modified surfactants with

Additional Supporting Information may be found in the online version of this article.
This article was published online on 26 June 2014. An error was subsequently identified. This notice is included in the online and print versions to indicate that both have been corrected 07 July 2014.

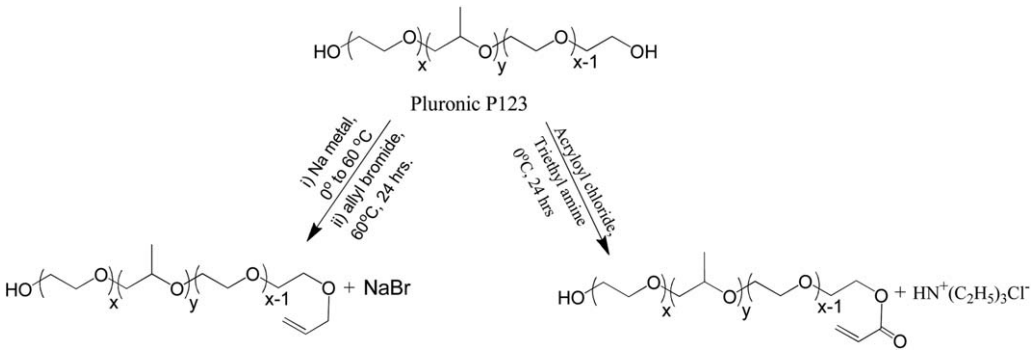

Scheme 1. General reaction sequence for allyl and acrylate end-group functionalization.

one another to create the continuous organic phase within and between the mesoporous silica particles, and network formation. In either case, the organic to inorganic composition ratios may be systematically varied in the final materials, as shown by several chemical, spectroscopic, and microscopic characterization methods described herein. The work is related to our recent published efforts involving the synthesis of novel biodegradable polymer structure-directing agents[28]; however, we demonstrate that simple chemistry on existing and commercially available polymeric templates can be used to create nanocomposite networks.

EXPERIMENTAL

Materials and Materials Characterization

Pluronic P123 was purchased from Sigma-Aldrich and used as received for functionalization reactions. Allyl bromide was purchased from Alfa Aesar and purified before use. Acryloyl chloride was purchased from Aldrich. All organic solvents were obtained from Pharmco-AAPER.

Surface area, pore size distribution, and pore volume of mesoporous silica were determined using nitrogen adsorption–desorption experiments on Nova2200e Quantachrome instruments. Surface area of mesoporous materials was calculated using Brunauer–Emmett–Teller (BET) model, and pore size distribution was determined with Barret–Joyner–Halenda (BJH) model. Transmission electron micrographs of mesoporous materials were acquired on JEOL JEM-2100 with Evex EDS.

Molecular weights were determined by gel permeation chromatography. The analyses were carried out using Agilent 1100 series equipped with refractive index detector. Polymer material (5 mg) was dissolved in 1 mL of tetrahydrofuran (THF). Poly(-ethylene glycol) (PEG) standards were used as calibration standards. THF was used as the eluting solvent at a flow rate of 1 mL/min, and two PLgel Mixed-C columns in series were used for the separation of polymeric materials. Polymer from composites was extracted with ethanol by refluxing composite with ethanol for 2 days. The mixture was filtered, and then, the solvent was removed by rotary evaporator.

A 600-MHz liquid NMR spectrometer (Varian) was used to determine ^{13}C-NMR (in $CDCl_3$) to determine the functionalized Pluronic P123 at 40°C at the spinning speed of 20 Hz. The solution temperature was equilibrated for 10 min before the measurements. Carbon solution spectra were acquired without Overhauser effects, a common method to increase the intensity of ^{13}C (lower gyromagnetic ratio) carbon signals by saturating the ^{1}H (higher gyromagnetic ratio) spins during the recycle delay. ^{13}C CP/MAS experiments were performed on the composites on 300-MHz solid-state NMR spectrometer (Bruker) equipped with 4-mm probe at a spinning speed of 5 kHz at room temperature. Percentage organic content was determined by heating the samples on TA instruments Hi-ResTGA2950 from room temperature to 600°C with the ramp rate of 20°C/min under air flow.

Small-angle X-ray scattering measurements were made in transmission with a SMax-3000 from Rigaku equipped with a Cu Kα source and a 10 cm × 10 cm 2D wire detector placed ~ 150 cm from the sample position. Silver behenate was used to determine the exact pixel to q ($q = 4\pi\sin\theta/\lambda$; θ = 0.5 × scattering angle, λ = 1.54 Å) conversion. Data were also corrected for pixel-to-pixel intensity variations as measured via exposing the plate to radiation emanating from a ^{55}Fe source.

Rheological tests were conducted using Rheometric Scientific RSA-II to measure storage and loss moduli using oscillating compression geometry. Parallel-plate fixtures of 10 mm were used, and measurements were made at room temperature with a gap size of 1.2 mm, dimensions which are in the range where such measurements are expected to give G' and G''.[29] Walberer and McHugh[29] described how force data from this type of measurement were converted to G' and G'' by making the lubrication approximation[29]; however, no instrumental inertia correction was required for this diameter plate according to instrument readings as well as data supplied by the manufacturer.

Synthesis of Allyl- and Acrylate-Functionalized Pluronic P123 (Denoted as aP123 and acryP123, Respectively)

Pluronic P123 was purchased from Sigma-Aldrich and used as such for functionalization reactions. Allyl bromide was purified before use. All organic solvents were obtained from Pharmco-AAPER. In a 250-mL two-necked flask, Pluronic P123 (1 mmol) was dissolved in 100 mL anhydrous THF in an inert atmosphere. The solution was cooled to 0°C and stirred at 400 rpm. The sodium metal (1.5 mmol), sliced into small pieces, was added to the above solution and heated at 60°C till all the sodium react with hydroxyl group. The allyl bromide (1.25 mmol) was then added dropwise into the reaction mixture and stirred at 60°C for 24 h. The precipitated sodium bromide

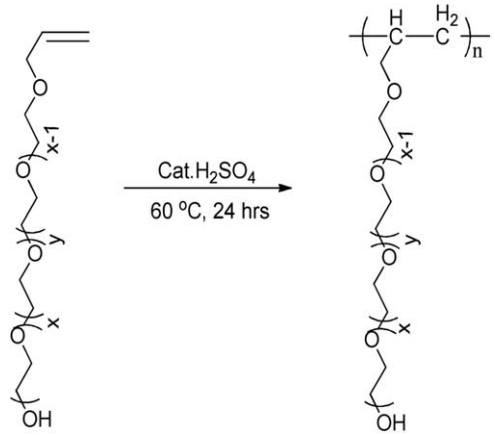

Scheme 2. Acid-catalyzed polymerization of allyl-functionalized chains.

was removed by filtration. The product was obtained by evaporating THF in a rotary evaporator and subsequently purified by extracting dichloromethane (DCM); the latter of which was removed in a rotary evaporator. The reaction scheme is shown in Scheme 1.

For acrylated P123 synthesis, to a 250-mL three-necked round-bottomed flask, Pluronic P123 (1 mmol) dissolved in 200 mL of anhydrous DCM was added. The temperature was lowered to 0°C, and acryloyl chloride (1.25 mmol) and triethyl amine (1 mmol) were added to the stirred solution. The reagents were reacted for 24 h. The triethyl ammonium chloride salt formed was separated by filtration. DCM was removed by rotary vaporization. The product was dried in a vacuum oven for 24 h at 60°C.

Synthesis of SBA-15 and SBA-15 Analogs

The molar composition for the synthesis of SBA-15 or SBA-15 type materials is TEOS : P123/**aP123** : HCl : H_2O = 1 : 0.016 : 5.54 : 182.82, where TEOS is tetraethylorthosilicate. In a typical synthesis, 4 g of P123 or **aP123** was dissolved in 30 mL of deionized water and stirred for 3 h at room temperature, and 112 mL of 2.133*M* HCl was added dropwise and kept under stirring for 2 h. The above solution was then heated to 40°C, and 9 g of TEOS was added dropwise and stirred for 20 h. The reaction mixture was kept at 100°C for 24 h under static conditions. The solution was divided into two equal quantities: first, half of the solution was kept at the same pH, and the other half kept was brought to neutral pH. The materials from each solution were washed with excess deionized water, dried overnight, and calcined at 550°C for 7 h using a temperature ramp of 1°C/min. As described in the text, TGA, XRD, pore volume, and BET analysis verified that crystalline mesoporous SBA-15 siliceous materials were formed in the presence of either P123 or **aP123**.

The molar composition for the synthesis of SBA-15 or SBA-15_acryP123 materials is TEOS : P123 (or acryP123) : HCl : H_2O = 1 : 0.016 : 5.54 : 182.82. In a typical synthesis, 4 g of P123 was dissolved in 30 mL of deionized water and stirred for 3 h at room temperature. About 112.16 mL of 2.133*M* of HCl was added dropwise and kept under stirring for 2 h. The above solution was then heated to 40°C, and 9 g of TEOS was added dropwise and stirred for 20 h. The reaction mixture was kept at 100°C for 24 h under static conditions. The mesoporous silica was filtered and rinsed with excess deionized water, dried on bench overnight, and calcined at 550°C for 7 h at the ramp of 1°C/min. As described in the text, TGA, XRD, pore volume, and BET analysis verified that crystalline mesoporous SBA-15 siliceous materials were formed in the presence of either P123 or **acryP123**.

Polymerization of aP123 and acryP123

Dilute H_2SO_4 was added to 1 g of aP123 in a catalytic amount, and the reaction mixture was heated to 60°C for 4 h; when polymerizing aP123 *in situ* to form the composite, the reaction time was increased to 24 h. The polymerization scheme is shown in Scheme 2. As described in the text (*vide infra*), GPC analysis of the polymeric component derived from aP123 revealed that a high-molecular-weight organic phase formed in the composite. Alternatively, the more reactive acrylate-functionalized P123 was polymerized via free radical methods as shown in Scheme 3, for either half an hour for the pure polymerization or for 10 h *in situ* to form the composite. To a 10-mL round-bottomed flask, 0.1 mmol of acryP123 was added. The flask was purged with ultrahigh pure argon to remove any oxygen. The temperature was then increased to 75–80°C. To this, 0.1 wt % (with respect to the organic content) azobis(isobutyronitrile) was added, and the reaction mixture was stirred for 30 min.

An essentially identical procedure was used when generating the composites or composite networks, except that the starting material was the dried as-synthesized SBA15_aP123 or SBA15_acryP123 materials. As synthesized, the starting composites contained 30 wt % **aP123** or **acryP123**, to which was added additional aP123 or acryP123 that would react along with the existing template molecules to generate the desired organic content composite. We successfully prepared 30–33, 50, 60, 80, and 90 wt % organic content composites or composite networks.

RESULTS AND DISCUSSION

Characterization of End-Group Functionalization in aP123 and acryP123

The 600-MHz solution ^{13}C-NMR spectrum of **aP123** is shown in Figure 1, following a typical conversion of the type shown in

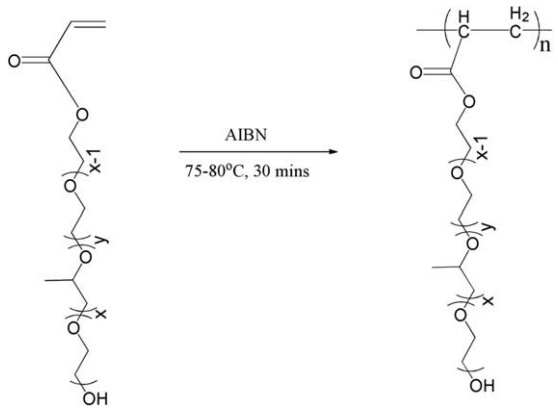

Scheme 3. Free-radical polymerization of acrylated-functionalized Pluronics.

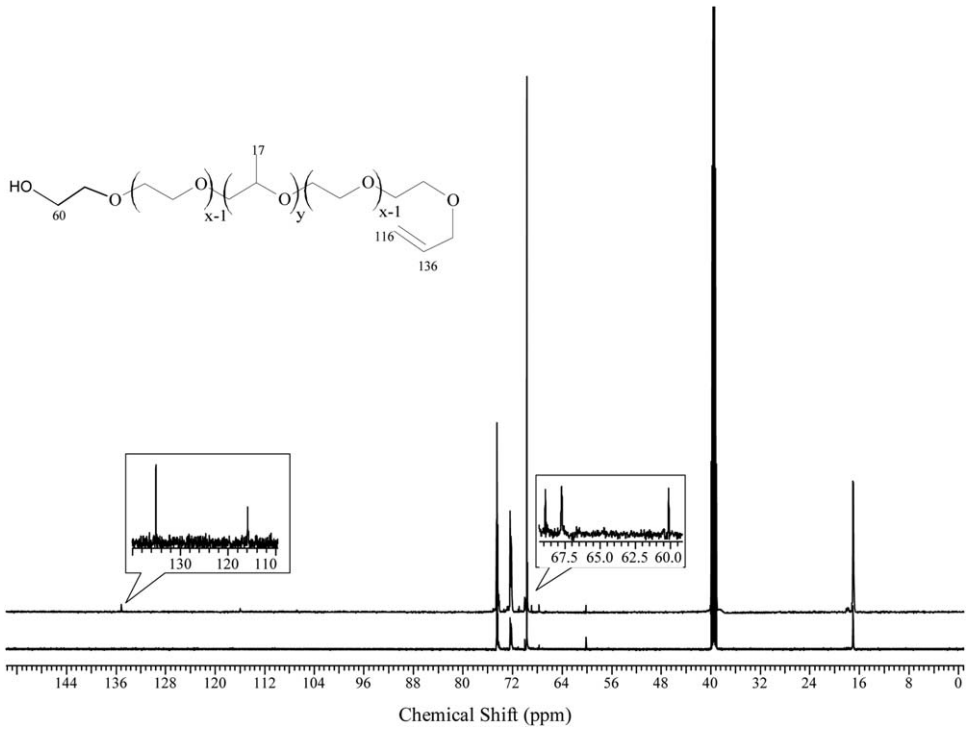

Figure 1. 600-MHz ^{13}C solution NMR spectrum acquired with ^{1}H decoupling of (bottom) pure P123 starting material and (top) allyl-functionalized **aP123** following reaction according to Scheme 1. Characteristic end-group signals, following reaction, are shown in the **aP123** inset.

the left side of Scheme 1. The spectrum was obtained with gated decoupling to minimize Overhauser effects. To preserve the structure-directing capabilities of P123, we targeted about 50% conversion of hydroxyl groups to allyl or acrylate groups in the respective allyl bromide or acryloyl chloride reactions. In other words, we wanted an average of one olefinic and one hydroxyl chain end per **aP123** or **acryP123** molecule. From Figure 1, which compares the starting P123 spectrum to the product **aP123**, one observes based on the relative intensities of the 60, 67, 116, and 136 ppm end-group peaks in the two spectra that this target was, on average, achieved. Note that the starting P123 in Figure 1 has only the characteristic 60-ppm end-group peak for the methylene group adjacent to the terminal hydroxyl.

Similarly, Figure 2 shows the comparable 600-MHz solution ^{13}C-NMR spectrum of acryP123 following a typical conversion of the type shown in the right side of Scheme 1. Again, the peaks in the inset demonstrate that on average, the reaction conditions yielded about 50% functionalization of the hydroxyl end groups on P123. Although not shown here, FTIR spectra clearly showed the acrylate carbonyl stretch at 1725 cm^{-1} after functionalization and purification.

Generating Mesoporous Silica from the Functionalized Nonionic Template/Macromers

Nonionic triblock copolymers based on polyethylene oxide and a central polypropylene oxide block, denoted here as PEO-PPO-PEO and commonly referred to by their Pluronic trade name, have garnered widespread attention for synthesis of SBA-15 mesoporous silicas.[7,18] Here, we use Pluronic P123, HO-$(PEO)_{20}$-$(PPO)_{70}$-$(PEO)_{20}$-H, as the template for SBA-15 formation, but use functionalization methods to convert one end group to a reactive olefinic moiety. Allyl bromide or acryloyl chloride, when reacted with P123 as described above in Scheme 1 and in the "Experimental" section, yields bifunctional **aP123** or **acryP123**, respectively. Reaction stoichiometries were selected to convert approximately one hydroxyl end group per P123 chain, as described in Figures 1 and 2. In this way, each modified P123 is rendered bifunctional and capable of subsequent polymerization through the olefinic end groups with surrounding template molecules, effectively as macromers. Given that the structure-directing characteristics of **aP123** and **acryP123** are not known, we first established that both nonionic surfactant macromers preserves P123's mesoporous silica structure-directing capabilities. Standard literature synthesis conditions[30] for SBA-15, using separate experiments P123 versus **aP123** versus **acryP123**, yielded mesoporous materials both before and after calcination, which are by all measures identical. Figure 3 compares the powder SAXS results from materials synthesized using the control P123 [Figure 3(a,d)], the modified **aP123** [Figure 3(b)], and **acryP123** [Figure 3(e)] prior to calcinations. Both the **aP123** and **acryP123** materials exhibit the specific diffraction peaks consistent with published SBA-15 topologies. Finally, Figure 3(c,f) shows the results for the diffraction in the polymerized composite, that is, after reaction in which the **aP123** or **acryP123** template macromers form the polymeric phase as shown in Schemes 2 and 3. Clearly, the mesoporous-ordered silica structure is preserved following polymerization. Additional information about the polymerization step is discussed below.

Although creating calcined mesoporous silicas is not the end goal, the BET surface areas and pore size distributions following

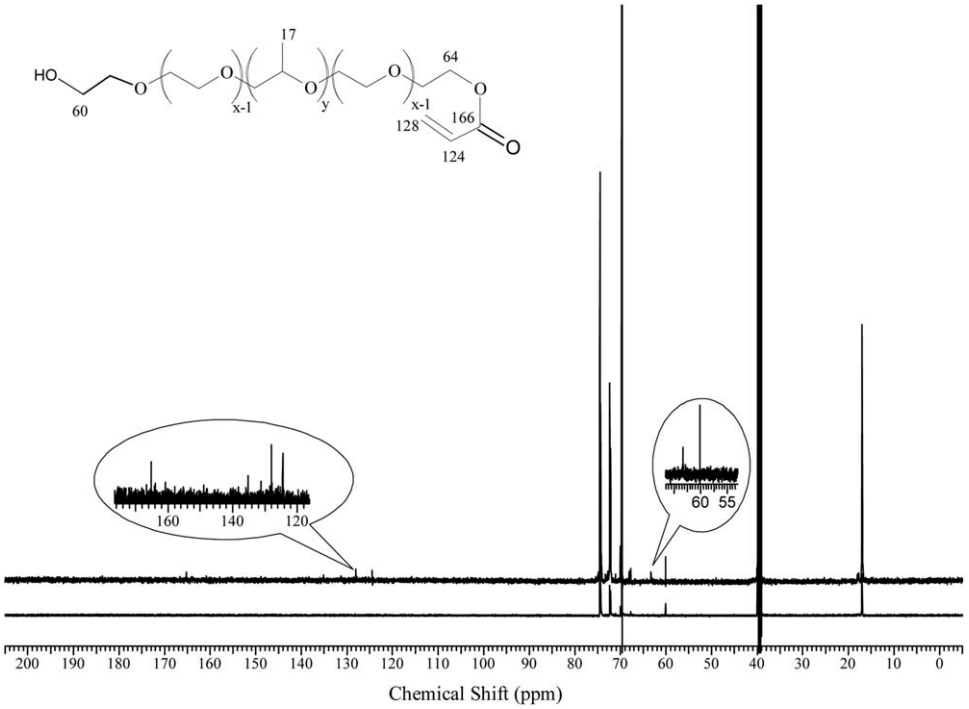

Figure 2. 600-MHz ^{13}C solution NMR spectrum acquired with ^{1}H decoupling of (bottom) pure P123 starting material and (top) acrylate-functionalized **acryP123** following reaction according to Scheme 1. End-group signals are shown in the **acryP123** inset, exhibiting the characteristic vinyl signals between 120 and 130 ppm.

calcination are key indicators that the modified templates still function as templates and compliment the SAXS data discussed above. Comparison of the surface area obtained for the calcined and dried **aP123/acryP123** SBA material with SBA-15 revealed that aP123 and acryP123 preserves the structure-directing capability. This result was replicated, and the essentially identical surface area for **aP123** SBA-15 was also observed for experiments in which the solution was neutralized to a pH = 7 prior to drying. However, separate experiments revealed that P123 modified to contain an olefinic group on both chain ends, that is, di-allyl with no hydroxyl groups, did not lead to SBA synthesis (*vide infra*). For **acryP123** template synthesis, the resulting mesoporous silica surface area was 930 m^2/g, again identical to that expected for SBA-15 structures synthesized from the

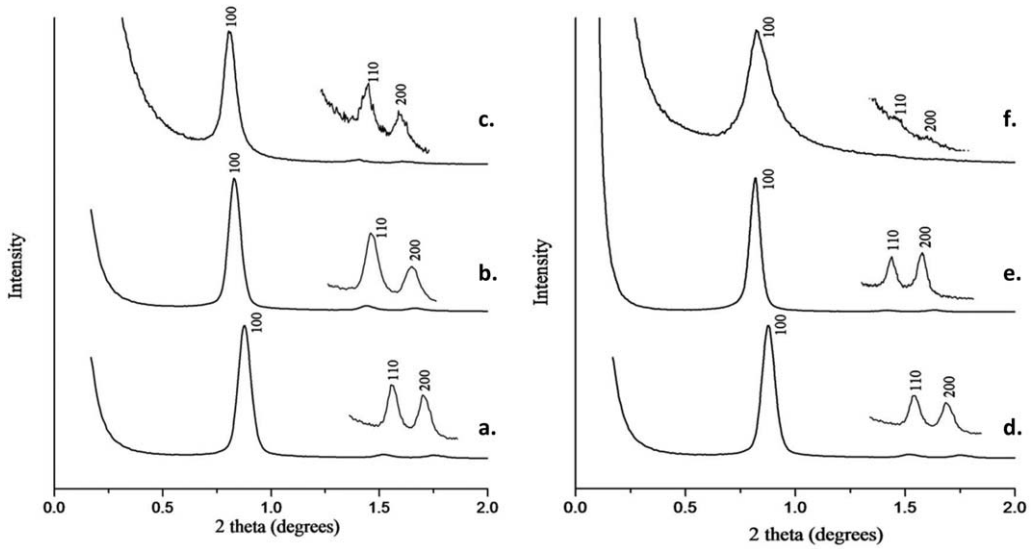

Figure 3. SAXS data of (a) SBA15P123; (b) SBA15_aP123; (c) SBA15_aP123 after polymerization of the aP123; (d) same as (a); (e) SBA15_acryP123; and (f) SBA15_acryP123 following polymerization. Diffractograms in (c) and (f) were acquired without calcination, and thus in the presence of the polymer product in and around the silica mesopores. There is a small change (0.84 vs. 0.87) in the position of the 100 peak relative to pure SBA; however, this corresponds to only a 0.4 nm difference in the total *d*-spacing.

Table I. Properties of Mesoporous Silica Prepared Using Pluronic P123, aP123, and acryP123. SAXS was Used to Determine the d-Spacing as Described in the Text. Pore Size Distributions and BET Surface Area were Determined Using N_2-Adsorption-Desorption Experiments[32].

Sample	d-spacing (100) (Å)	BET Surface area (m^2/g)	Pore size (Å)
SBA15_P123	100.40	945	32
SBA15_acryP123	113.10	930	30
SBA15_aP123	106.50	921	33

unfunctionalized P123. Average pore diameters and pore size distributions were measured via BJH N_2 adsorption/desorption isotherm experiments[25] and were essentially identical for P123, **aP123**, and **acryP123**-templated silicas (Figure 4 and Table I). Adsorption–desorption isotherms of dried and calcined aP123/acryP123 SBA material show Type IV hysteresis typical of mesoporous silica and similar to SBA-15.[31–33] Additionally, similar average pore diameters and *d*-spacings for calcined and dried aP123/acryP123 SBA material clearly indicate that anchoring monomeric unit (allyl/acrylic) in Pluronic P123 does not alter the ability to form micelles in the aqueous environment or to template crystallization of ordered mesoporous.

Figure 5(a–c) shows representative TEM results for SBA-15 prepared from P123 in the traditional manner (SBA15_P123), SBA-15 prepared from **aP123** (SBA15_aP123), and SBA-15 prepared from **acryP123** (SBA15_acryP123). In all three cases, the characteristic 4-nm hexagonally arrayed channels are observed. Again, the goal with these detailed characterizations is to show that modified surfactant macromers preserve SBA-15 templating, while providing the added postsynthetic polymerization capability needed to form a continuous organic phase both within and outside of the mesoporous silica particles. Note that the scale for Figure 5(c) is twice that shown in Figure 5(a,b).

Polymerizing the Reactive Template Macromers to form Composites and Composite Networks

Following the synthesis of SBA-15 with either **aP123** or **acryP123**, the reactive templates can be polymerized *in situ*, as depicted in Schemes 2 and 3, but now with the added feature that polymerization begins within the SBA-15 channels resulting in higher molecular weight chains that percolate through and outside of the channels. Although the details of the two chemistries are slightly different, specifically with respect to crosslinking between chains as will be discussed further below, the basic reaction scheme is similar for each template and is shown in Figure 6.

To confirm that polymerization took place starting from the **aP123** template, the resulting polymeric fraction was extracted by refluxing the final organic/silica composite material in 50°C ethanol for 48 h. As controls, GPC analysis of pure P123 and **aP123** prior to any reaction is shown in Figure 7(a,b). Monodisperse PEG standards were used to calibrate the GPC, and the resulting elution time for the pure P123 agreed with its known molecular weight (5700 g/mol). In another control experiment, **aP123** was reacted with sulfuric acid at the same concentration to ensure that their polymerization occurred, and the high-molecular-weight peak (broad signal near 6 min) shown in Figure 7(c) indicates that the chemistry leads to polymerization of the **aP123** macromers. Finally, Figure 7(d) shows the GPC result for the polymeric fraction extracted from the final organic/silica composite material after SBA crystallization and polymerization. The results are similar to Figure 7(c), indicating that higher molecular weight species (up to 115,000 g/mol) are formed from the reaction of the **aP123** structure-directing agent molecules in the composite. TGA analysis of the washed and dried composite, after extraction of the polymer used to generate Figure 7(d), revealed that 13 wt % of the polymer remained in the SBA channels after extraction, consistent with the formation of higher molecular species like those depicted in Scheme 2.

Figure 7(d) also shows unreacted **aP123**, which is consistent with what is known about the relatively low reactivity of the allyl end group. However, as this was the first proof-of-principle example, and clearly reaction does occur in the composite to essentially the same extent as the polymerization of pure **aP123**, we believe that the result represents the general methodology accurately. In addition, rheological measurements clearly showed improved stress/strain properties after polymerization and also improvements relative to just pure polymer. More importantly, these results motivated us to pursue the more reactive acrylate end-group approach, as described below.

Because of the relatively low reactivity of the allyl end groups, acrylated P123 (**acryP123**) was pursued as an improved synthesis method. GPC analysis of the organic fraction generated by polymerizing the **acryP123** template was not possible, as network formation occurred quickly. As a control, polymerization of pure **acryP123** was also investigated. In each case, networks were formed as verified by solvent-swelling experiments. Although not shown here for brevity, images comparing pure **acryP123** and composites derived from polymerizing **acryP123** in the mesoporous host showed obvious swelling behavior. Importantly, no swelling occurred for the pure **acryP123**; however, polymerized **acryP123** exhibits a large (ca. 300–400%) volume-swelling ratio. The organic/inorganic composites prepared from the polymerization of the **acryP123** all exhibited significant solvent swelling, and none were soluble in any common solvent. Given the increased reactivity of the acrylate chemistry, some of the polymer chains are functionalized on each end, which leads to the network formation. This is depicted schematically in Scheme 4.

The SBA15_aP123 and SBA15_acryP123 composites, as synthesized, contain 30–33 wt % organic content as defined by the initial surfactant/TEOS reaction stoichiometry. However, adding additional **aP123** or **acryP123** at the time the polymerization catalyst is added yields final products with much higher organic content. In this way, we have systematically and repeatedly generated composites with up to 10 wt % silica content, as verified by TGA analysis on the final washed and dried products. Representative TGA results for the composites made from SBA15_acryP123 are shown in Figure 8, with silica contents of 70, 20, and 10 wt %. Figure 8(a) also shows the control experiment for

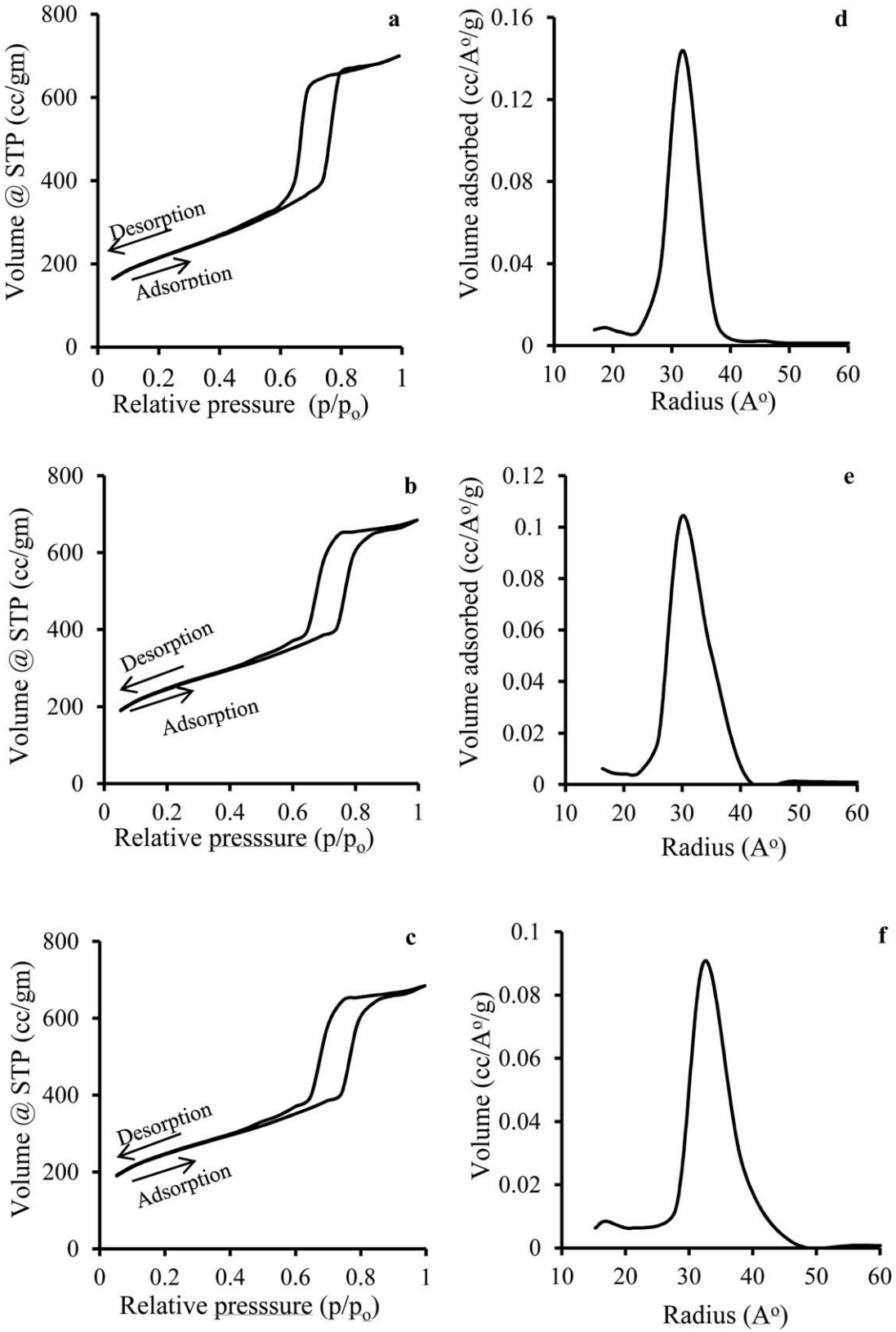

Figure 4. Nitrogen adsorption–desorption curves (on left) and pore size distributions (on right) of SBA15_P123 (a and d); SBA15_acryP123 (b and e); and SBA15_aP123 (c and f), respectively.

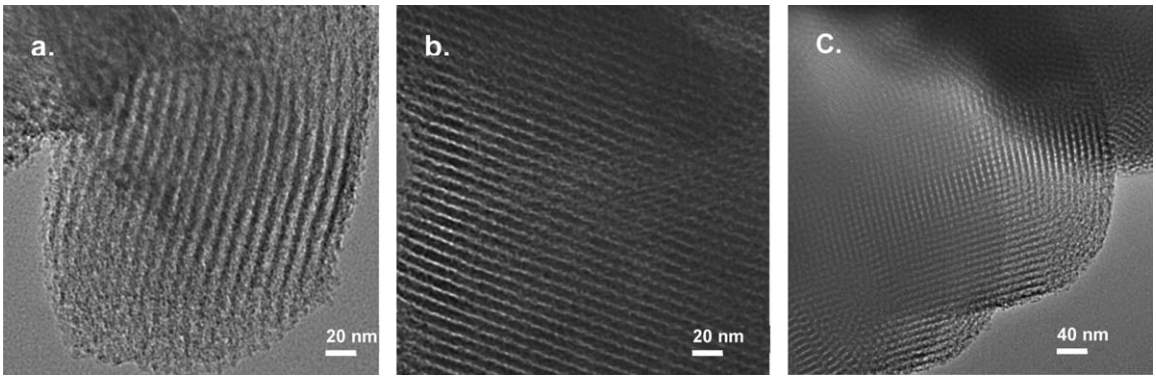

Figure 5. TEM micrographs of (a) SBA15P123, (b) SBA15_aP123, and (c) SBA15_acryP123. Images (a) and (b) are shown at ×100,000 magnification, and image (c) is shown at ×50,000 magnification.

the polymerization of pure **acryP123**; similar results were obtained for **aP123**-generated composites.

Solid-state ^{13}C MAS and CP/MAS NMR experiments on the washed and dried **aP123** and **acryP123** composites unequivocally indicate that polymerization of the functionalized templates takes place. Figure 9 compares the ^{13}C CP/MAS data for the **aP123** molecules in as-synthesized SBA-15 versus that for the **aP123**/SBA-15 composite generated by polymerization. The peak at 31 ppm in Figure 9(b) indicates that polymerization through the olefinic end groups has occurred in the composite synthesis, thereby generating a series of aliphatic CH_2 groups in the chain. The single-pulse ^{13}C MAS spectrum in Figure 9(c) confirms this assignment; however, importantly, the intensity of the 31 ppm peak is significantly reduced. As cross-polarization (CP) preferentially emphasizes constrained environments with larger static dipolar couplings, this much larger peak intensity in the CP experiment, relative to the other signals in the CP spectrum, is expected as these groups are near a long-chain branch point in the chain (Scheme 2). This fact also explains why the unreacted allyl end groups are not observed in Figure 9(a), as they are too mobile to cross-polarize.

Figure 10 shows a similar set of CP/MAS results for the acryP123/SBA-15 system, and as the data shown in Figure 9, it is revealed that polymerization of the acryP123 templates takes place inside and around the SBA-15. The 30 wt % organic content composite in Figure 10(b) exhibits a complex, broad signal

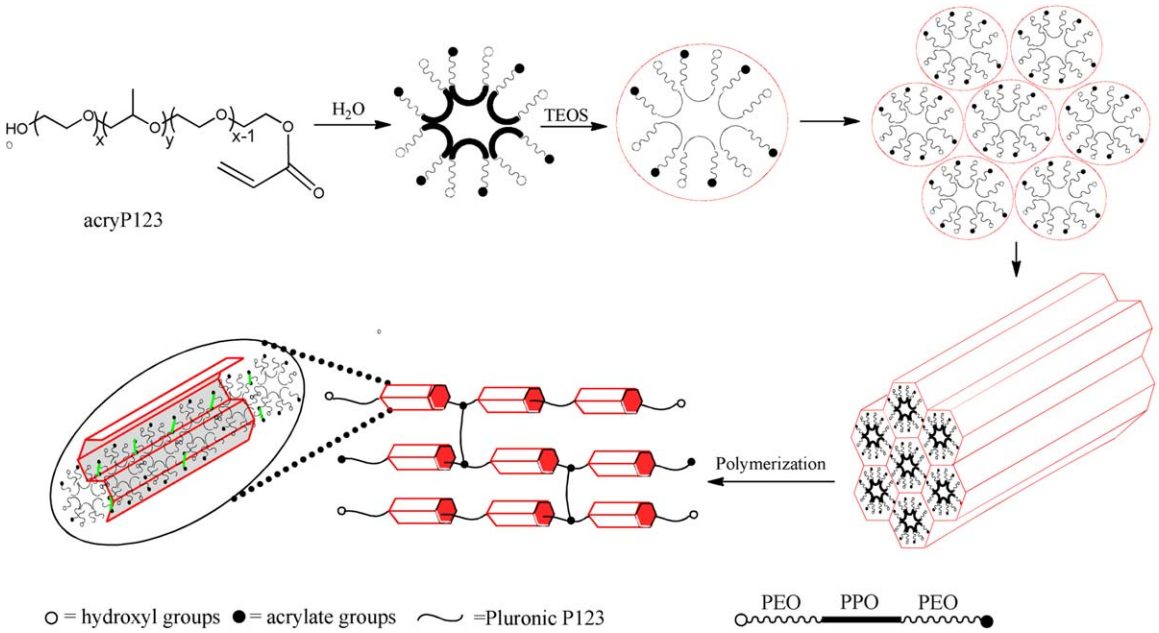

Figure 6. General schematic representation of self-assembly and synthesis of polymer composites using either the **acryP123** or **aP123** template macromers; the acryP123 structure is shown. Polymerization between macromers occurs within and outside of the SBA particles. The small orange hexagons in the last frame of the reaction scheme are an idealized representation of individual SBA particles in the network, which of course are not regularly arrayed as shown. Crosslinking to form networks occurred in the acryP123 system, but not in the aP123 system, most likely due to the increased reactivity of the small fraction of macromers that contain acrylate groups on both chain ends under free radical polymerization conditions. [Color figure can be viewed in the online issue, which is available at wileyonlinelibrary.com.]

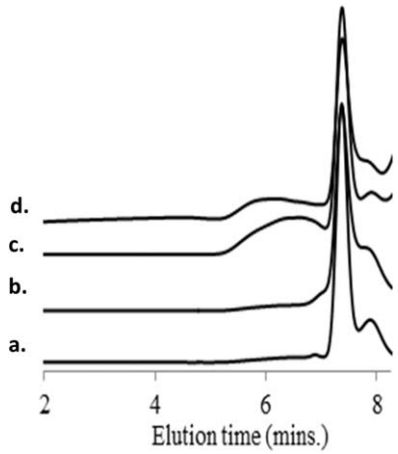

Figure 7. GPC chromatograms of (a) pure P123, (b) aP123, (c) polymerized pure aP123, and (d) polymer extracted from the composite following polymerization of aP123 template molecules *in situ*. No change in molecular weight was observed for control experiments involving pure P123 in the same acid-catalyzed reaction. GPC flow rates were 1 mL/min.

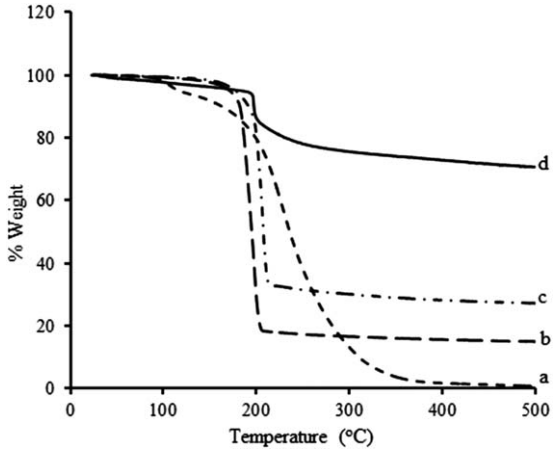

Figure 8. TGA results for polymer nanocomposites made using acryP123 composites with (a) 0, (b) 10, (c) 20, and (d) 70 wt % silica content.

for the carbonyl group, ranging from 164 to 180 ppm, which is absent in the unpolymerized sample [Figure 10(a)] and is also not visible in the higher organic content composite in Figure 10(c). This indicates that the polymerization does occur between adjacent macromers within the constrained SBA-15 channels in the as-prepared composite, prior to adding any additional acryP123, which is important as polymer chain connectivity through the SBA-15 channels is required if the organic phase is to be continuous throughout the material. The carbonyl signals are not observed in the CP spectrum of 70 wt % composite as the bulk-averaged behavior of organic phase is much more mobile than the 30% (organic fraction) material; the latter of which has the majority of its chain density within the SBA-15 channels.

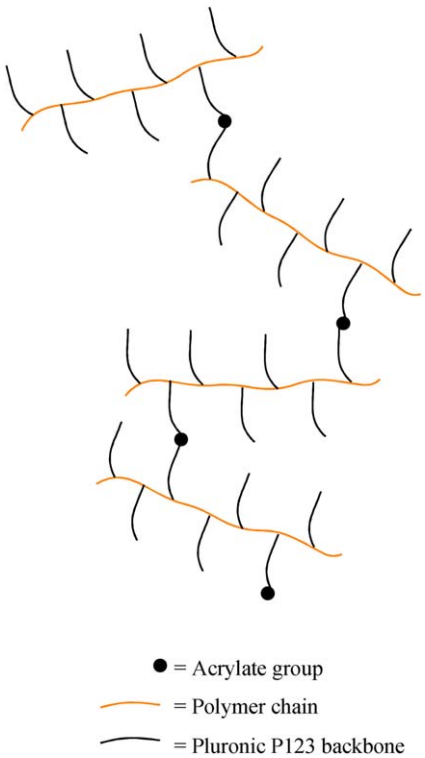

Scheme 4. Route for network formation via doubly-functionalized allyl macromers. [Color figure can be viewed in the online issue, which is available at wileyonlinelibrary.com.]

Interparticle versus Intraparticle Polymerizations and Physical Properties

The minimum organic content in the composite, as defined by the initial stoichiometry required to crystallize SBA-15 from solution, is 30 wt % **aP123** or **acryP123**. For the **aP123** system, adding more **aP123** at the point of catalytic acid addition can easily increase the organic content; however, our experiments

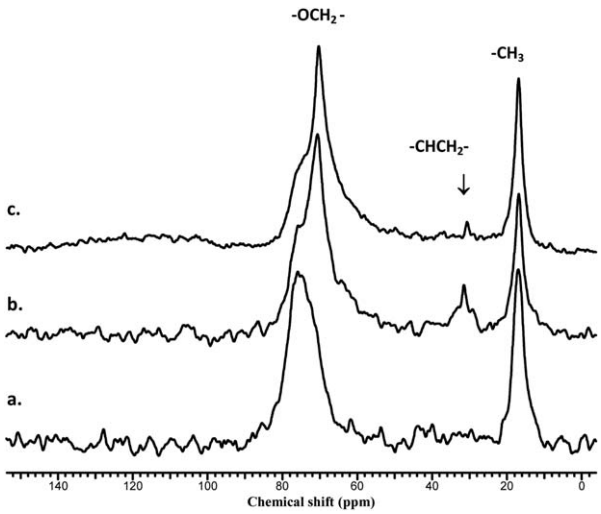

Figure 9. Solid-state $^{1}H \rightarrow {}^{13}C$ CP/MAS spectra for (a) the aP123 template in uncalcined SBA-15 following synthesis but prior to polymerization and (b) the organic fraction generated by polymerizing the aP123 structure-directing agents inside and around the SBA-15 following crystallization. (c) Single-pulse MAS spectrum obtained at the same spinning speed. The arrow denotes the new aliphatic CH/CH_2 moieties formed from the reaction. Note the significantly reduced 31-ppm intensity in image (c) versus image (b).

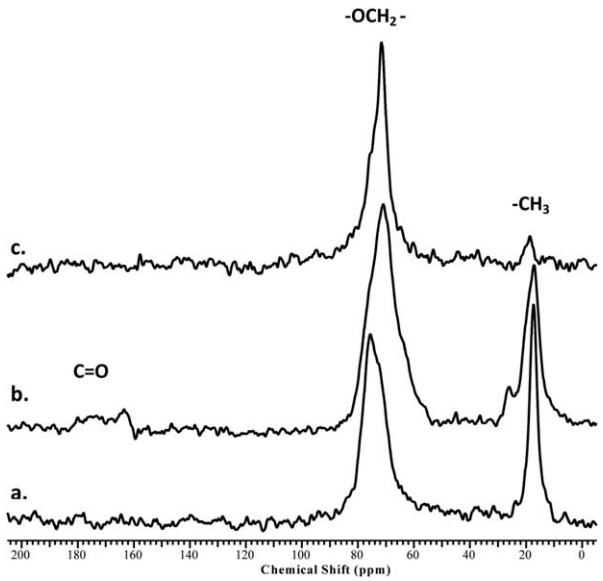

Figure 10. Solid-state $^{1}H \rightarrow {}^{13}C$ CP/MAS spectra for (a) the acryP123 template in uncalcined SBA-15 following synthesis but prior to polymerization, (b) the organic fraction generated by polymerizing the acryP123 structure-directing agents inside and around the SBA-15 following crystallization, corresponding to a 30 wt % polymer composite, and (c) same starting material as in (a) but with additional acryP123 added prior to polymerization, resulting in a polymerized composite with 70 wt % organic fraction.

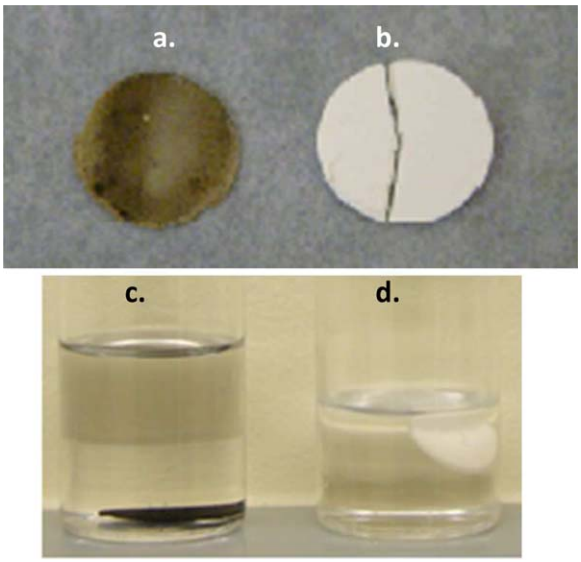

Figure 11. Pellets formed from (a) polymerized aP123/SBA-15 composite versus (b) versus aP123/SBA-15 without the polymerization step. Both pellets contain about 30–33 wt % organic content. (c) Pellet from polymerized composite in CH_2Cl_2, at the bottom of the vial, and (d) the corresponding unpolymerized control pellet floating near the surface. The two pellets were placed in each solvent container at exactly the same time, which was 1 min prior to taking the photo. [Color figure can be viewed in the online issue, which is available at wileyonlinelibrary.com.]

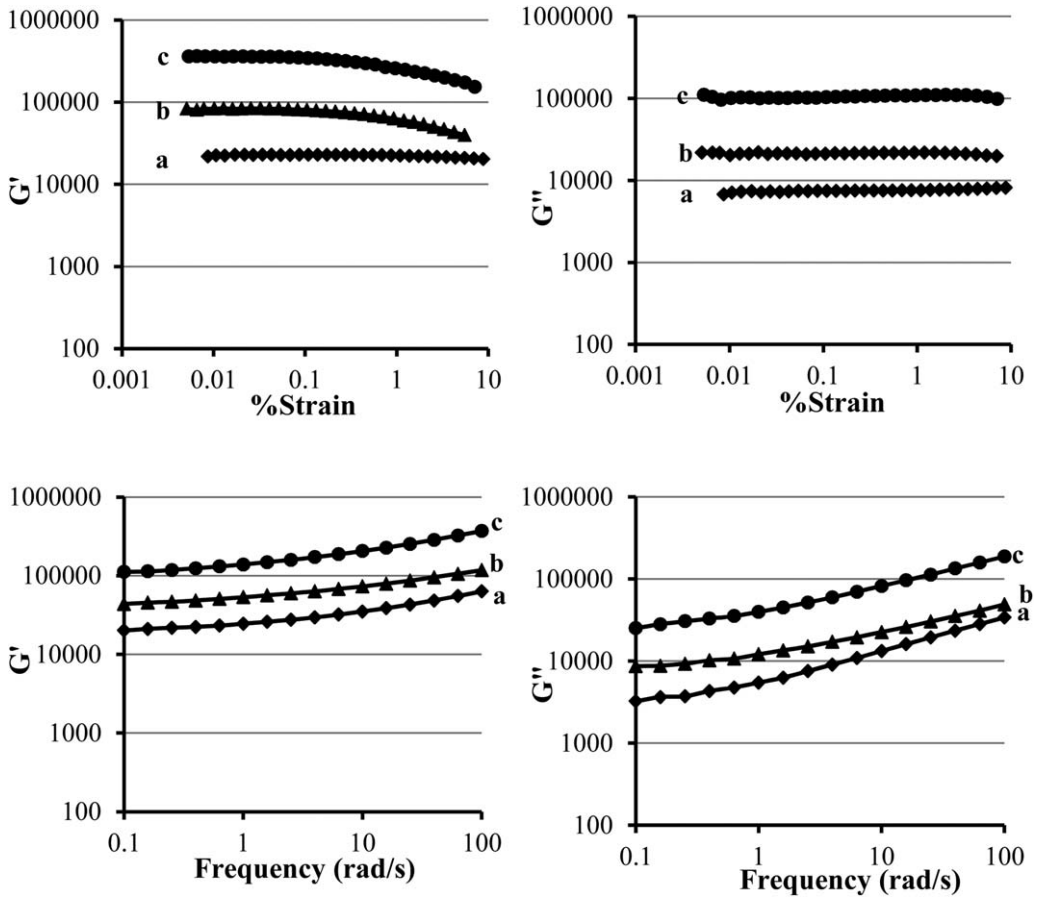

Figure 12. Storage moduli (G') and loss moduli (G'') collected from strain sweep (top row) and frequency sweep (bottom row) of acryP123 nanocomposite networks with (a) 0, (b) 10, and (c) 20 wt % silica content.

indicate that even at this lower limit, polymerization occurs between **aP123** macromers both inside and outside of the SBA particle channels. Polymerization outside of the channels is required for interparticle connectivity and true composite properties. To assess the degree to which interparticle polymerization occurred, two different materials were pressed into cylindrical pellets at room temperature using a Carver press. The two samples were chemically identical, composed of the **aP123**/SBA-15 mixture following crystallization, washing, and drying. However, one of the two samples was polymerized, whereas the other was not polymerized. Figures 7 and 9 prove that polymerization occurs for **aP123**, and if that polymerization is only limited to the interior of the mesoporous silica, then pellets formed from unpolymerized (but still filled with unreacted **aP123**) versus polymerized material should exhibit essentially identical physical properties. Figure 11(a,b) compares the images of the pellets formed from each material at 3000-psi plate pressure and room temperature. The unpolymerized material, which exhibits the white color expected for silica, does not form a stable pellet at this pressure, as indicated by the large crack through the bulk material. Indeed, the pellet crumbled when removed from the mold. In contrast, the darker colored polymerized composite pellet forms a tough, stable pellet that may be removed and handled. Similar results were obtained in multiple experiments. If the plate pressure was increased to 5000 psi, then an apparently stable pellet could be made from the unpolymerized sample; however, its surface was chalky and easily removed by simply rubbing one's finger across it. More importantly, solvent-exposure experiments demonstrated that interparticle connectivity occurred in the polymerized **aP123**/SBA-15 sample. When the 5000-psi unpolymerized pellet was dropped into DCM, it immediately rose to the surface while simultaneously releasing visible air bubbles. After a few minutes, no more bubbles were observed, and the pellet settled to the bottom of the beaker. However, the 3000-psi polymerized **aP123**/SBA-15 pellet, as that shown in Figure 10(a), immediately settled to the bottom of beaker filled with DCM, and no air bubbles were ever released. The pellet was stable in the solution for several hours, with little change in its shape or color. The unpolymerized pellet, formed at the higher 5000-psi pressure, developed multiple cracks and began to disintegrate after only 1 h in solvent. Figure 11(c,d) shows the polymerized versus unpolymerized **aP123**/SBA-15 pellets in DCM. Altogether, these experiments prove that polymerization occurs between the particles, and not just within their intracrystalline channels, even for the minimum 33 wt % organic content. Similar results were also observed in case of acryP123/SBA-15.

Similarly, mechanically stable pellets were formed from the polymerized 30 wt % **acryP123**/SBA-15 system at 3000 psi, but not from the unpolymerized control, and their images were compared with those shown for the aP123 system in Figure 11. However, because the **acryP123**/SBA-15 composites have cross-linking within the continuous organic phase, their physical properties at higher organic content are different than the **aP123** system. As shown previously, they swell in solvents, whereas the aP123 systems dissolve, and they have a rubbery texture in the solid state.

Strain- and frequency-sweep rheological experiments on acryP123 nanocomposites were performed at room temperature using a parallel-plate RSAII rheometer from TA instrument. Linear viscoelastic regimes (LVRs) were experimentally determined at 1 Hz frequency with variable strain measurements (0.01–10%). The top row of Figure 12 shows that the LVR of the nanocomposites exist between 0.01 and 0.15% strain. In accordance with the strain sweep data, frequency sweep data were then collected at 0.15% strain and are shown in the bottom row of Figure 12. The frequency sweep data indicate that the modulus increases as the increase in the content of silica of polymer nanocomposites. In addition, the storage and loss moduli of the nanocomposites are essentially independent of the frequency, suggesting that true networks are formed in the composites.

CONCLUSIONS

A novel route to organic/inorganic composite materials has been introduced, which uses end-group functionalization of commercially available structure-directing agents that enable self-assembly of intimately mixed nanocomposites. Using allyl- or acrylate-functionalized P123 as a template, we have shown that crystallization of SBA-15 is preserved, but that following the crystallization, the template readily polymerizes to form a composite containing high-molecular-weight polymer filling and surrounding the SBA-15 crystallites in an intimately mixed arrangement. The acrylate-functionalized P123 route also introduces network properties to the nanocomposites. The overall organic-to-inorganic ratio can be varied in a systematic manner, and increases in moduli of the polymer nanocomposites were observed with increasing silica content.

ACKNOWLEDGMENTS

This work was supported by the National Science Foundation Division of Materials Research through grant DMR-0756291. The authors thank Professor Brian Grady, University of Oklahoma, for assistance with X-ray diffraction experiments.

REFERENCES

1. Ooi, Y. S.; Bhatia, S. *Microporous Mesoporous Mater.* **2007**, *102*, 310.
2. Pasqua, L.; Cundari, S.; Ceresa, C.; Cavaletti, G. *Curr. Med. Chem.* **2009**, *16*, 3054.
3. Zornoza, B.; Irusta, S.; Tellez, C.; Coronas, J. *Langmuir* **2009**, *25*, 5903.
4. Kiba, S.; Suzuki, N.; Okawauchi, Y. *Chem. Asian J.* **2010**, *5*, 2100.
5. Moller, K.; Bein, T.; Fischer, R. X. *Chem. Mater.* **1998**, *10*, 1841.
6. Zhang, F. A.; Lee, D. K.; Pinnavaia, T. *J. Polymer* **2009**, *50*, 4768.
7. Ji, X. L.; Hampsey, J. E.; Hu, Q. Y.; He, J. B.; Yang, Z. Z.; Lu, Y. F. *Chem. Mater.* **2003**, *15*, 3656.

8. Lin, Y. S. Y.; Radu, D. R.; Han, M. K.; Deng, W.; Kuroki, S.; Shanks, B. H.; Pruski, M. *J. Am. Chem. Soc.* **2002**, *124*, 9040.
9. Sasidharan, M.; Mal, N. K.; Bhaumik, A. *J. Mater. Chem.* **2007**, *17*, 278.
10. Merkel, T. C.; Freeman, B. D.; Spontak, R. J.; He, Z.; Pinnau, I.; Meakin, P.; Hill, A. *J. Science* **2002**, *296*, 519.
11. Merkel, T. C.; Freeman, B. D.; Spontak, R. J.; He, Z.; Pinnau, I.; Meakin, P.; Hill, A. *J. Chem. Mater.* **2003**, *15*, 109.
12. Zou, H.; Wu, S.; Shen, J. *Chem. Rev.* **2008**, *108*, 3893.
13. Audouin, F.; Blas, H.; Pasetto, P.; Beaunier, P.; Boissière, C.; Sanchez, C.; Save, M.; Charleux, B. *Macromol. Rapid Commun.* **2008**, *29*, 914.
14. Anwander, R.; Nagl, I.; Zapilko, C.; Widenmeyer, M. *Tetrahedron* **2003**, *59*, 10567.
15. Lunn, J. D.; Shantz, D. F. *Chem. Mater.* **2009**, *21*, 3638.
16. Kruk, M.; Dufour, B.; Celer, E. B.; Kowalewski, T.; Jaroniec, M.; Matyjaszewski, K. *Macromolecules* **2008**, *41*, 8584.
17. Perez, L. D.; Lopez, J. F.; Orozco, V. H.; Kyu, T.; Lopez, B. L. *J. Appl. Polym. Sci.* **2005**, *111*, 2229.
18. Hoffmann, F.; Cornelius, M.; Morell, J.; Fröba, M. *Angew. Chem. Int. Ed. Engl.* **2006**, *45*, 3216.
19. Burkett, S. L.; Sims, S. D.; Mann, S. *Chem. Commun.* **1996**, 1367.
20. Macquarrie, D. *J. Chem. Commun.* **1996**, 1961.
21. Lim, M. H.; Blanford, C. F.; Stein, A. *J. Am. Chem. Soc.* **1997**, *119*, 4090.
22. Tong, X.; Tang, T.; Zhu, N.; Feng, Z. L.; Huang, B. T. *Chem. J. Chin. Univ.* **2002**, *23*, 306.
23. Tong, X.; Tang, T.; Zhang, Q. L.; Feng, Z. L.; Huang, B. T. *J. Appl. Polym. Sci.* **2002**, *83*, 446.
24. Tong, X.; Tang, T.; Feng, Z. L.; Huang, B. T. *J. Appl. Polym. Sci.* **2002**, *86*, 3532.
25. Houel, A.; Galy, J.; Charlot, A.; Gerard, J. F. *J. Appl. Polym. Sci.* **2014**, *131*, 39830.
26. Li, L.; Yang, G. *J. Appl. Polym. Sci.* **2011**, *120*, 1957.
27. Hsieu, G. H.; Kuo, W. J.; Huang, Y. P.; Feng, R. *J. Polymer* **2000**, *41*, 2813.
28. Patil, N.; Kelsey, J.; Grady, B. P.; White, J. L. *Polymer* **2014**, *55*, 2332.
29. Walberer, J. A.; McHugh, A. J. *J. Rheol.* **2001**, *45*, 187.
30. Zhao, D.; Feng, J.; Huo, Q.; Melosh, N.; Fredrickson, G. H.; Chmelka, B. F.; Stucky, G. D. *Science* **1998**, *279*, 548.
31. Tompsett, G. A.; Krogh, L.; Griffin, D. W.; Conner, W. C. *Langmuir* **2005**, *21*, 8214.
32. Barrett, E. P.; Joyner, L. G.; Halenda, P. P. *J. Am. Chem. Soc.* **1951**, *73*, 373.
33. Maglara, E.; Kaminski, R.; Conner, W. C. In Characterization of Porous Solids IV; McEnaney, B., Mays, T. J., Rouquerol, J., Rodrigues-Reinoso, F., Sing, K. S. W., Unger, K. K.; Royal Society of Chemistry: London, **1997**. p 25.